Vol 18 No 11, November 2009
1674-1056/2009/18(11)/4769-08

Chinese Physics B

© 2009 Chin. Phys. Soc.
and IOP Publishing Ltd

An efficient numerical approach to electrostatic microelectromechanical system simulation*

Li Pu(李 普)†

College of Mechanical Engineering, Southeast University, Nanjing 211189, *China*

(Received 7 June 2008; revised manuscript received 17 April 2009)

Computational analysis of electrostatic microelectromechanical systems (MEMS) requires an electrostatic analysis to compute the electrostatic forces acting on micromechanical structures and a mechanical analysis to compute the deformation of micromechanical structures. Typically, the mechanical analysis is performed on an undeformed geometry. However, the electrostatic analysis is performed on the deformed position of microstructures. In this paper, a new efficient approach to self-consistent analysis of electrostatic MEMS in the small deformation case is presented. In this approach, when the microstructures undergo small deformations, the surface charge densities on the deformed geometry can be computed without updating the geometry of the microstructures. This algorithm is based on the linear mode shapes of a microstructure as basis functions. A boundary integral equation for the electrostatic problem is expanded into a Taylor series around the undeformed configuration, and a new coupled-field equation is presented. This approach is validated by comparing its results with the results available in the literature and ANSYS solutions, and shows attractive features comparable to ANSYS.

Keywords: microelectromechanical systems, self-consistent, boundary element method

PACC: 0710C, 0670M

1. Introduction

Recently there has been growing interest in the development of MEMS systems. Although there are many microelectromechanical system designs in which piezoelectric, thermal, and magnetic actuations are used, the most popular approach in present-day MEMS designs is to use electrostatic forces to move micromachined parts.[1] Designers of such MEMS devices need efficient simulation tools to investigate design alternatives. Computational analysis of MEMS requires a self-consistent solution of the coupled interior mechanical domain and the exterior electrostatic domain.[1−6] Conventionally, the finite element method (FEM) is employed to perform the mechanical analysis, and the boundary element method (BEM) is employed to compute the surface charge densities.[2] The main steps of the self-consistent solution are organized as follows. The mechanical analysis is performed by discretizing the structural or the mechanical domain into nodes and elements. A finite element analysis is then performed by using the electrostatic pressure as Neumann boundary conditions to compute the structural displacements. Once the displacement is computed, the geometry of the structure or the conductor is updated. Electrostatic analysis is performed on the updated geometry by discretizing the surface of the conductor into panels or elements. The BEM is then used to compute the surface charge density on each panel. Once the surface charge densities are known, the new electrostatic pressure is computed. The mechanical and the electrostatic analyses are repeated until an equilibrium state is computed. So a major difficulty with computational efficiency is the need to update the geometry and remesh the surface of the structures before an electrostatic analysis is performed during each iteration. When the structure undergoes large deformation, the updating and remeshing are also needed before a mechanical analysis is performed during each iteration.

In order to improve computational efficiency, many techniques are presented. We can identify two groups of these techniques on this topic. In the first group, the structure undergoes large deformation. Aluru, White, Li and Paulino[1,2,4,7−9] presented some techniques to improve computational efficiency. In the second group, the structure deformation is small. Many techniques (Reduced-order Model)[10−14] have been developed based on using the linear mode shapes of a device as basis functions. The deformed structural

*Project supported by the National Natural Science Foundation of China (Grant No 50675034) and the Natural Science Foundation of Jiangsu Province of China (Grant No SBK200920386).

†E-mail: seulp@seu.edu.cn

domain is described by a factored sum of the mode shape for efficiently solving the coupled-field problems. But updating the geometry and remeshing the boundary surface of the structures are still necessary before an electrostatic analysis is performed during each iteration. In the present paper, small deformation is referred to as the deflection of the microbeam. It is a precondition for the Taylor series expansion for derivation. But for the electrostatic field, the effect of the deflection of the microbeam is significant.

In the present paper, we present a new efficient numerical approach to MEMS device fast simulation in the small deformation case. The approach is also based on the linear mode shapes of a microstructure as basis functions. A boundary integral equation for the electrostatic problem is expanded into a Taylor series around the undeformed configuration. A new coupled-field equation is derived. The surface charge densities on the deformed geometry can be computed directly without updating the geometry and remeshing the boundary surface of the structures. So the major advantage of the approach is that the computational efficiency is improved effectively.

The rest of this paper is organized as follows. In Section 2 the mechanical analysis and the electrostatic analysis are described and a new coupled-field equation is presented. In Section 3, the new approach is validated by comparing its results with the results available in Ref.[8] and ANSYS solutions (ESSLOV), and attractive features comparable to ANSYS software are indicated. Finally, some conclusions are drawn in Section 4.

2. Coupled-field analysis

A clamped-clamped microbeam actuator shown in Fig.1 serves as an example in this paper, but the approach can be extended slightly to three-dimensional problems.

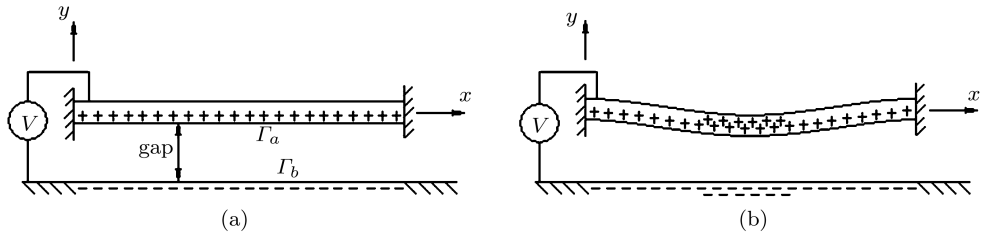


Fig.1. Schematic representation of a clamped-clamped microbeam actuator, where (a) is for charge distribution induced by applied voltage and (b) is for deformed structure with charge redistribution.

2.1. Microbeam equation

The equation that governs the transverse deflection $y(x)$ in Fig.1 is written as

$$EI\frac{\partial^4 y}{\partial x^4} = f(x, y, V), \tag{1}$$

where E is the Young's modulus, I is the moment of inertia of the cross section, $y(x)$ is the microbeam deflection curve, V is the dc voltage, $f(x, y, V)$ is the electrostatic force acting on the microbeam, Γ_a and Γ_b are the surfaces of two conductors. In the small deflection case, using modal techniques,[15] $y(x)$ can be expressed as

$$y(x) = \sum_{m=1}^{N} c_m \phi_m(x), \tag{2}$$

where $\phi_m(x)$ are the mth linear undamped mode shape of the microbeam at the undeformed position, and c_m are the generalized coordinates, N is the number of selected modes. Substituting expression (2) into Eq.(1), and multiplying each term by a normal mode $\phi_i(x)$, integrating along the beam length and calling upon the orthogonality property[15] of the mode shapes leads to

$$c_i \cdot k_i = \int_0^L \phi_i(x) f(x, y(x), V)\,\mathrm{d}x, \quad \text{for } i = 1, \ldots, N, \tag{3}$$

where $k_i = EI\int_0^L \phi_i(x)\dfrac{\partial^4 \phi_i(x)}{\partial x^4}\,\mathrm{d}x$ is the generalized stiffness corresponding to mode i.

2.2. Electrostatic analysis: boundary element method

The governing equation along with the boundary conditions for the exterior electrostatic problem is given by[7]

$$\nabla^2 U(x,y) = 0 \quad \text{in} \quad \Omega, \tag{4}$$

$$U(x,y) = V \quad \text{on} \quad \Gamma_a, \tag{4a}$$

$$U(x,y) = 0 \quad \text{on} \quad \Gamma_b, \tag{4b}$$

where $U(x,y)$ is the potential function, Ω is the domain external to two conductors. A boundary integral equation for the electrostatic problem is given by[7,16]

$$U(\boldsymbol{p}) = \int_{\Gamma} G(\boldsymbol{p},\boldsymbol{q})\sigma(\boldsymbol{q})\,\mathrm{d}\Gamma(\boldsymbol{q}) + C, \tag{5}$$

$$\int_{\Gamma} \sigma(\boldsymbol{q})\,\mathrm{d}\Gamma(\boldsymbol{q}) = C_{\mathrm{T}}, \tag{6}$$

where $\boldsymbol{p}$ is the position vector of field point p; $\boldsymbol{q}$ is the position vector of source point q; σ is the unknown surface charge density; $\Gamma = \Gamma_a + \Gamma_b$; G is the Green's function. In two dimensions, $G(\boldsymbol{p},\boldsymbol{q}) = -\ln|\boldsymbol{p}-\boldsymbol{q}|/2\pi\varepsilon$, where $|\boldsymbol{p}-\boldsymbol{q}|$ is the distance between the source point q and the field point p, ε is the permittivity of the free space, C_{T} is the total charge of the system ($C_{\mathrm{T}} = 0$) and C is an unknown variable which needs to be computed. The constant C is introduced because the potential U at infinity is not zero for 2D electrostatic problems. In a classical boundary element method, the surface is discretized into panels and the surface charge density is assumed to be constant on each panel. The centroid of each panel is taken as the collocation point and the value of the potential and the surface charge density at the collocation point represent the value of the potential and the surface charge density on the panel, respectively. The boundary integral equation can be rewritten as

$$U(\boldsymbol{p}_i) = \sum_{j=1}^{K} \sigma_j \cdot \int_{\Gamma_j} \left[-\frac{\ln|\boldsymbol{p}_i - \boldsymbol{q}_j|}{2\pi\varepsilon}\right] \mathrm{d}\Gamma(\boldsymbol{q}_j) + C,$$
$$i = 1, 2 \ldots K, \tag{7}$$

$$\sum_{j=1}^{K} \sigma_j \Gamma_j = C_{\mathrm{T}}, \tag{8}$$

where $\boldsymbol{p}_i$ is the position vector of field point p on the ith panel, K is the number of panels, Γ_j is the length of the jth panel, σ_j is the unknown charge density for the kth panel and $\boldsymbol{q}_j$ is the position vector of source point q on the jth panel. Equations (7) and (8) can be rewritten in a matrix form as

$$\bar{\boldsymbol{M}}\bar{\sigma} = \bar{\boldsymbol{V}}, \tag{9}$$

where $\bar{\boldsymbol{M}}$ is a $(K+1)\times(K+1)$ coefficient matrix, $\bar{\boldsymbol{V}}$ and $\bar{\boldsymbol{\sigma}}$ are the $(K+1)\times 1$ right-hand side and unknown vectors, respectively. The elements in the coefficient matrix are given by

$$\begin{aligned}
&\bar{M}(i,j) = \int_{\Gamma_j} \left[-\frac{\ln|\boldsymbol{p}_i - \boldsymbol{q}_j|}{2\pi\varepsilon}\right] \mathrm{d}\Gamma(\boldsymbol{q}_j),\\
&i,j = 1, \ldots K,\\
&\bar{M}(K+1,j) = \int_{\Gamma_j} \mathrm{d}\Gamma(q_j), \quad j = 1, \ldots K,\\
&\bar{M}(i,K+1) = 1, \quad i = 1, \ldots K,\\
&\bar{M}(K+1,K+1) = 0,
\end{aligned} \tag{10}$$

$$\begin{aligned}
\bar{\boldsymbol{V}}_{(K+1)\times 1} &= [V_1 \;\; V_2 \;\; \ldots \;\; V_K \;\; C_{\mathrm{T}}]^{\mathrm{T}},\\
\bar{\boldsymbol{\sigma}}_{(K+1)\times 1} &= [\sigma_1 \;\; \sigma_2 \;\; \ldots \;\; \sigma_K \;\; C]^{\mathrm{T}}.
\end{aligned} \tag{11}$$

Note that the elements in coefficient matrix $\boldsymbol{M}$ are written with respect to the deformed position of the structure. In conventional self-consistent methods, almost all the elements in matrix $\boldsymbol{M}$ should be regenerated before an electrostatic analysis is performed during each iteration, so updating the geometry and remeshing the boundary surface of the structures are necessary. Clearly, this is inefficient.

Considering the deflection of the microbeam, $\boldsymbol{p}_i = \hat{\boldsymbol{p}}_i + \Delta\boldsymbol{p}_i$, $\boldsymbol{q}_j = \hat{\boldsymbol{q}}_j + \Delta\boldsymbol{q}_j$, and $\Gamma_j = \hat{\Gamma}_j + \Delta\Gamma_j$, where $\hat{\boldsymbol{p}}_i$ and $\hat{\boldsymbol{q}}_j$ are the the position vector of the field point and the position vector of the source undeformed position, $\Delta\boldsymbol{p}_i$ and $\Delta\boldsymbol{q}_j$ are $\boldsymbol{q}_j$ are the displacement vectors, $\hat{\Gamma}_j$ is the length of the jth panel at the undeformed position, $|\boldsymbol{p}_i - \boldsymbol{q}_j| = \sqrt{(\hat{x}_{p_i} - \hat{x}_{q_j})^2 + (\hat{y}_{p_i} + \Delta y_{p_i} - \hat{y}_{q_j} - \Delta y_{q_j})^2}$, and $\Gamma_j = \sqrt{(\hat{x}_{j_1} - x_{j_2})^2 + (\hat{y}_{j_1} + \Delta y_{j_1} - \hat{y}_{j_2} - \Delta y_{j_2})^2}$, where $(\hat{x}_{p_i}, \hat{y}_{p_i})$ and $(\hat{x}_{q_j}, \hat{y}_{q_j})$ are the coordinates of the field point and the source point at the undeformed position, $(\hat{x}_{j_1}, \hat{y}_{j_1})$ and $(\hat{x}_{j_2}, \hat{y}_{j_2})$ are the two coordinates of extreme points of the jth panel at the undeformed position. Equations (7) and (8) can be rewritten as

$$U(\boldsymbol{p}_i)=\sum_{j=1}^{K}\sigma_j\cdot\int_{\hat{\Gamma}_j+\Delta\Gamma_j}\left[-\frac{\ln|\hat{\boldsymbol{p}}_i+\Delta\boldsymbol{p}_i-\hat{\boldsymbol{q}}_j-\Delta\boldsymbol{q}_j|}{2\pi\varepsilon}\right]\times \mathrm{d}\Gamma(\hat{\boldsymbol{q}}_j+\Delta\boldsymbol{q}_j)+C,\quad i=1,2\ldots K, \tag{12}$$

$$\sum_{j=1}^{K}\sigma_j(\hat{\Gamma}_j+\Delta\Gamma_j)=C_{\mathrm{T}}. \tag{13}$$

In Eqs.(7) and (12), the line integral defined in the jth element is evaluated numerically by using a standard Gaussian quadrature.[17] The Gaussian integration is performed over the interval $-1\le\xi\le 1$. So a local coordinate system[17] is introduced at the jth element, and the line integral in the global coordinates is mapped onto the interval $[-1,1]$. The Jacobian of the transformation is $|J(\xi)|=(\hat{\Gamma}_j+\Delta\Gamma_j)/2$. In the case of small deformation, $\mathrm{d}\Gamma(\hat{\boldsymbol{q}}_j+\Delta\boldsymbol{q}_j)=\mathrm{d}\xi(\hat{\Gamma}_j+\Delta\Gamma_j)/2\approx\mathrm{d}\Gamma(\hat{\boldsymbol{q}}_j)$, thus we expand the terms on the right-hand side of Eq.(12) and the terms on the left-hand side of Eq.(13) into a Taylor series around $(\hat{\boldsymbol{p}}_i,\ \hat{\boldsymbol{q}}_j)$ and $\hat{\Gamma}_j$ up to the first order, respectively, and rewrite Eqs.(12) and (13) as

$$\begin{aligned}U(\boldsymbol{p}_i)\approx&\left\{\sum_{j=1}^{K}\sigma_j\cdot\int_{\hat{\Gamma}_j}\left[-\frac{\ln|\hat{\boldsymbol{p}}_i-\hat{\boldsymbol{q}}_j|}{2\pi\varepsilon}\right]\mathrm{d}\Gamma(\hat{\boldsymbol{q}}_j)+C\right\}+\sum_{j=1}^{K}\frac{\sigma_j}{2\pi\varepsilon}\cdot\left[\int_{\hat{\Gamma}_j}\frac{-\hat{y}_{p_i}+\hat{y}_{q_j}}{|\hat{\boldsymbol{p}}_i-\hat{\boldsymbol{q}}_j|^2}\mathrm{d}\Gamma(\hat{\boldsymbol{q}}_j)\right]\cdot\Delta y_{p_i}\\&+\sum_{j=1}^{K}\frac{\sigma_j}{2\pi\varepsilon}\cdot\left[\int_{\hat{\Gamma}_j}\frac{\hat{y}_{p_i}-\hat{y}_{q_j}}{|\hat{\boldsymbol{p}}_i-\hat{\boldsymbol{q}}_j|^2}\mathrm{d}\Gamma(\hat{\boldsymbol{q}}_j)\right]\cdot\Delta y_{q_j},\quad\text{for}\quad i=1,2\ldots K,\end{aligned} \tag{14}$$

$$\sum_{j=1}^{K}\sigma_j(\hat{\Gamma}_j+\Delta\Gamma_j)\approx\sum_{j=1}^{K}\sigma_j\left(\hat{\Gamma}_j+\frac{\hat{y}_{j_1}-\hat{y}_{j_2}}{\hat{\Gamma}_j}\cdot\Delta y_{j_1}+\frac{\hat{y}_{j_2}-\hat{y}_{j_1}}{\hat{\Gamma}_j}\cdot\Delta y_{j_2}\right)=C_{\mathrm{T}}. \tag{15}$$

Using modal analysis techniques,[15] the deformations Δy_{p_i}, Δy_{q_j}, Δy_{j_1} and Δy_{j_2} can be expressed as

$$\begin{aligned}\Delta y_{p_i}&=\sum_{m=1}^{N}c_m\phi_m(\hat{x}_{p_i}),\quad \Delta y_{q_j}=\sum_{m=1}^{N}c_m\phi_m(\hat{x}_{q_j}),\\ \Delta y_{j_1}&=\sum_{m=1}^{N}c_m\phi_m(\hat{x}_{j_1}),\quad \Delta y_{j_2}=\sum_{m=1}^{N}c_m\phi_m(\hat{x}_{j_2}).\end{aligned} \tag{16}$$

Substituting Eq.(16) into Eqs.(14) and (15), we obtain

$$\boldsymbol{M}_{(K+1)\times(K+1)}\bar{\boldsymbol{\sigma}}_{(K+1)\times1}=\bar{\boldsymbol{V}}_{(K+1)\times1}, \tag{17}$$

where $\bar{\boldsymbol{V}}_{(K+1)\times1}=\left[\begin{array}{cccc}V_1 & V_2 & \ldots & V_K\ C_{\mathrm{T}}\end{array}\right]^{\mathrm{T}}$, $\bar{\boldsymbol{\sigma}}_{(K+1)\times1}=\left[\begin{array}{cccc}\sigma_1 & \sigma_2 & \ldots & \sigma_K\ C\end{array}\right]^{\mathrm{T}}$,

$$\boldsymbol{M}_{(K+1)\times(K+1)}=\left[\begin{array}{cc}\hat{M}_{K\times K}+c_1\boldsymbol{M}^{[1]}_{K\times K}+c_2\boldsymbol{M}^{[2]}_{K\times K}\ldots+c_N\boldsymbol{M}^{[N]}_{K\times K} & \boldsymbol{I}_{K\times1}\\ \hat{\boldsymbol{A}}_{1\times K}+c_1\boldsymbol{A}^{[1]}_{1\times K}+c_2\boldsymbol{A}^{[2]}_{1\times K}\ldots+c_N\boldsymbol{A}^{[N]}_{1\times K} & 0_{1\times1}\end{array}\right],\quad \boldsymbol{I}_{K\times1}=\left[\begin{array}{cccc}1 & 1 & \ldots & 1\end{array}\right]^{\mathrm{T}},$$

$$\hat{\boldsymbol{M}}_{K\times K}(i,j)=\int_{\hat{\Gamma}_j}\left[-\frac{\ln|\hat{\boldsymbol{p}}_i-\hat{\boldsymbol{q}}_j|}{2\pi\varepsilon}\right]\mathrm{d}\Gamma(\hat{\boldsymbol{q}}_j),\quad\text{for}\ \ i,j=1,2,\ldots,K\,,\quad \hat{\boldsymbol{A}}_{1\times K}(1,j)=\hat{\Gamma}_j,\quad\text{for}\ \ j=1,2,\ldots,K\,,$$

$$\boldsymbol{M}^{[n]}_{K\times K}(i,j)=\frac{\phi_n(\hat{x}_{p_i})\cdot(-\hat{y}_{p_i}+\hat{y}_{q_j})+\phi_n(\hat{x}_{q_j})\cdot(\hat{y}_{p_i}-\hat{y}_{q_j})}{2\pi\varepsilon}\cdot\left[\int_{\hat{\Gamma}_j}\frac{1}{|\hat{\boldsymbol{p}}_i-\hat{\boldsymbol{q}}_j|^2}\mathrm{d}\Gamma(\hat{\boldsymbol{q}}_j)\right],\quad\begin{array}{l}\text{for}\ \ i,j=1,2,\ldots,K,\\ n=1,2,\ldots,N,\end{array}$$

$$\boldsymbol{A}^{[n]}_{1\times K}(1,j)=\frac{\hat{y}_{j_1}-\hat{y}_{j_2}}{\hat{\Gamma}_j}\cdot\phi_n(\hat{x}_{j_1})+\frac{\hat{y}_{j_1}-\hat{y}_{j_2}}{\hat{\Gamma}_j}\cdot\phi_n(\hat{x}_{j_2}),\quad\text{for}\ \ j=1,2,\ldots,K;\ n=1,2,\ldots,N.$$

Note that submatrixes $\hat{\boldsymbol{M}}_{K\times K}, \boldsymbol{M}^{[1]}_{K\times K}, \boldsymbol{M}^{[2]}_{K\times K} \ldots \boldsymbol{M}^{[N]}_{K\times K}$ and $\hat{\boldsymbol{A}}_{1\times K}, \boldsymbol{A}^{[1]}_{1\times K}, \boldsymbol{A}^{[2]}_{1\times K} \ldots \boldsymbol{A}^{[N]}_{1\times K}$ are computed at the undeformed position of the microbeam, the generalized coordinates $c_1, c_2, \ldots c_N$ represent the deformation of the microbeam. So updating the geometry and remeshing the boundary surface of the structures are not necessary, only $c_1, c_2, \ldots c_N$ should be updated before an electrostatic analysis is performed during each iteration, thus the computation time can be saved effectively as compared with the conventional Eqs.(9) and (10). It should be stressed that the integration in $\boldsymbol{M}^{[n]}_{K\times K}(i,j)$ exhibits a singular behaviour when $i = j$. The value can be evaluated by using an indirect method.[17,18]

2.3. Electrostatic-structural coupled equation

The electrostatic force on the sth panel of the microbeam is given by[4]

$$h_s = \frac{\sigma_s}{2\varepsilon} n_s, \tag{18}$$

where h_s is the force per unit length and n_s is the outward normal of the sth panel at the deformed position. In the case of small deformation, Eq.(1) can be rewritten as

$$c_i \cdot k_i = \int_0^L \phi_i(x) f(x, y(x), V)\,\mathrm{d}x \approx \sum_{s=1}^{K_1} \phi_i \left(\frac{\hat{x}_{s_1} + \hat{x}_{s_2}}{2} \right) \frac{\sigma_s}{2\varepsilon} \hat{\Gamma}_s, \quad \text{for} \quad i = 1, \ldots, N, \tag{19}$$

where K_1 is the number of boundary elements in Γ_a. Rewrite Eqs.(17) and (19) into a matrix form as

$$\begin{bmatrix} \boldsymbol{S}_{N\times N} & \boldsymbol{0}_{N\times(K+1)} \\ \boldsymbol{0}_{(K+1)\times 1} & \boldsymbol{M}_{(K+1)\times(K+1)} \end{bmatrix} \begin{bmatrix} \bar{\boldsymbol{c}}_{N\times 1} \\ \bar{\boldsymbol{\sigma}}_{(K+1)\times 1} \end{bmatrix} = \begin{bmatrix} \boldsymbol{I}_{N\times 1} \\ \bar{\boldsymbol{V}}_{(K+1)\times 1} \end{bmatrix}, \tag{20}$$

where

$$\boldsymbol{S}_{N\times N}(i,j) = \begin{cases} k_i \cdot \left[\sum_{s=1}^{K_1} \phi_i \left(\dfrac{\hat{x}_{s_1} + \hat{x}_{s_2}}{2} \right) \dfrac{\sigma_s}{2\varepsilon} \hat{\Gamma}_s \right]^{-1}, & i = j\,, \\ 0, & i \neq j\,, \end{cases}$$

$$\bar{\boldsymbol{c}}_{N\times 1} = \begin{bmatrix} c_1 & c_2 & \ldots & c_N \end{bmatrix}^{\mathrm{T}}, \quad \boldsymbol{I}_{N\times 1} = \begin{bmatrix} 1 & 1 & \ldots & 1 \end{bmatrix}^{\mathrm{T}}.$$

$\bar{\boldsymbol{c}}_{N\times 1}$ and $\bar{\boldsymbol{\sigma}}_{(K+1)\times 1}$ are unknown variables. The coupled-field equation (20) can be solved easily by using the self-consistent method.

3. Case study

In order to validate the new approach in this paper, a MATLAB code is used to solve Eq.(20). For comparison, the static deflections of three fixed-fixed microbeam cases[8] are calculated as a function of the dc voltage varying from 0 V to the value of pull-in voltage. The three cases have three different gaps; their numerical results provided by large deformation analysis are available in Ref.[8]. ANSYS (ESSOLV command[16]) is also used to simulate the three cases. In ANSYS, the FEM is employed to perform the electrostatic analysis; morphing and remeshing techniques are also used to update the finite element mesh in the non-structural region to coincide with the structural deflection and recursively cycle between the field solution and structural solution.[16] In the following section, we compare the results obtained from the new approach with the results available in Ref.[8] and the results of ANSYS as well.

The fixed-fixed microbeam[8] is 100 μm long, 50 μm wide, 1 μm thick, and is positioned at 0.5 μm, 2 μm, 4 μm above the ground plane, separately. The microbeam is discretized into 40 boundary elements, the ground plane is discretized into 50 boundary elements. Figure 2 shows the peak deflection results of the microbeam with a gap of 0.5 μm with using one-, two-, and four-mode discretizations respectively. For comparison, the results available in Ref.[8] and the results of ANSYS are also plotted in Fig.2. The FEM model in ANSYS is also two dimensional. Figures 3 and 4 show the peak deflection results of the

microbeam with a gap of 2 μm and a gap of 4 μm, respectively.

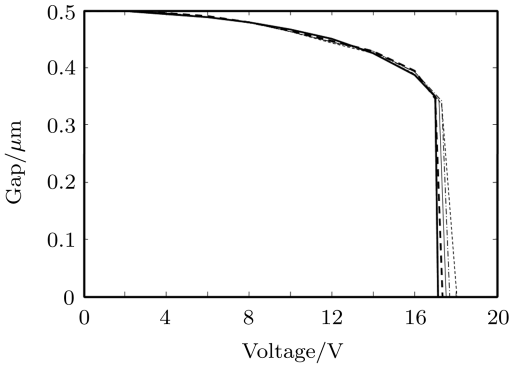


Fig.2. Comparison between new approach results, results available from Ref.[8] and ANSYS results for a fixed-fixed microbeam with a gap of 0.5 μm. Heavy solid line —— results cited from Ref.[8]; heavy dashed line——ANSYS results; fine dashed line——1-mode results; fine dash dot line——2-mode results; fine solid line——4-mode results.

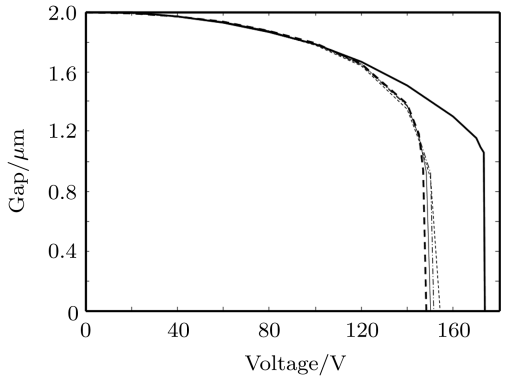


Fig.3. Comparison between new approach results, results available from Ref.[8] and ANSYS results for a fixed-fixed microbeam with a gap of 2 μm. Heavy solid line—— results cited from Ref.[8]; heavy dash line——ANSYS results; fine dashed line——1-mode results; fine dash dot line——2-mode results; fine solid line——4-mode results.

In Fig.2, it is clear that the results (heavy solid line) available in Ref.[8] and the ANSYS results (heavy dashed line) are in good agreement with each other due to the small deformation of the microbeam. Also, the 4-mode solution (fine solid line) of the new approach is very close to the ANSYS results and is clearly more accurate than the 1-mode solution (fine dash line) and the 2-mode solution (fine dash dot line), especially in pull-in voltage. All five curves are very close before pull-in voltage. The displacement of the microbeam at pull-in voltage is very close to the 1/3 gap.

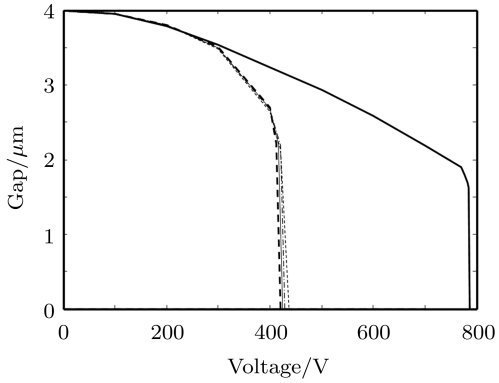


Fig.4. Comparison between new approach results, results available from Ref.[8] and ANSYS results for a fixed-fixed microbeam with a gap of 4 μm. Heavy solid line—— results cited from Ref.[8]; heavy dash line——ANSYS results; fine dashed line——1-mode results; fine dash dot line——2-mode results; fine solid line——4-mode results.

In Fig.3, for a large gap 2 μm, it is clear that the pull-in voltage is significantly different between the results available in Ref.[8] and the ANSYS results. But the 1-mode, 2-mode and 4-mode solutions of the new approach are still close to the ANSYS results. The 4-mode solution is clearly more accurate than the 1-mode and the 2-mode solutions, especially at pull-in voltage. When the voltage is less than 120 V, all five curves are in good agreement with each other due to the small deformation of the microbeam. Figure 4 is similar to Fig.3, but the difference in pull-in voltage is even larger between the results available in Ref.[8] and the ANSYS results. The results obtained from our new approach are still very close to the ANSYS results.

In order to examine the computational efficiency of the new approach in this paper, another MATLAB code is used to solve the problems in the three cases based on the conventional self-consistent method. Comparisons between the new approach (4-mode) and the conventional method are summarized in Tables 1–3 separately. Note that the iterations of the new approach are almost the same as those of the conventional method, but the new approach is fast compared with the conventional method.

Table 1. Comparison between results from new approach and conventional method for a beam with a gap of 0.5 μm.

bias voltage/V	# iterations		CPU time/s	
	the conventional method	the new approach	the conventional method	the new approach
2	4	4	10.5	11.0
4	5	5	13.0	13.1
6	5	5	13.2	13.1
8	6	6	13.8	13.6
10	6	7	14.2	14.0
12	8	8	16.1	15.5
14	9	8	20.6	17.0
16	12	12	24.3	18.9
17	19	19	33.5	21.1
17.35	27	26	40.4	25.4

Table 2. Comparison between results from new approach and conventional method for a beam with a gap of 2 μm.

bias voltage/V	# iterations		CPU time/s	
	the conventional method	the new approach	the conventional method	the new approach
20	4	4	14.4	14.6
40	4	4	14.8	14.8
60	5	5	15.2	15.1
80	6	6	17.5	17.1
100	7	7	18.3	17.8
120	8	8	26.0	24.7
140	10	9	31.1	28.5
145	15	14	40.3	33.0
147	21	20	49.0	36.6
149	28	29	60.5	40.1

Table 3. Comparison between results from new approach and conventional method for a beam with a gap of 4 μm.

bias voltage/V	# iterations		CPU time/s	
	the conventional method	the new approach	the conventional method	the new approach
100	4	4	16.5	16.7
200	5	5	20	19.8
300	8	9	24	23.0
400	19	19	51.5	35.3
412	25	25	69.6	42.2

4. Conclusions

In this paper, we introduce a new efficient numerical approach for MEMS device fast simulation in the case of small deformation. The approach is also based on the linear mode shapes of a microstructure as basis functions. Additionally, a boundary integral equation for the electrostatic problem is expanded into a Taylor series around the undeformed configuration, a new coupled-field equation is derived, and the surface charge densities on the deformed geometry can be computed directly without updating the geometry and remeshing the boundary surface of the structures. So the major advantage of the approach is that computational efficiency is improved effectively. This approach is validated by comparing its results with the results available in Ref.[8] and ANSYS software solutions, and shows attractive features comparable to ANSYS software.

References

[1] Aluru N R and White J 1999 *IEEE J. Microelectromech. Syst.* **8** 299

[2] Li G and Aluru N R 2003 *IEEE Trans. Computer-Aided Design* **22** 1228

[3] Senturia S D 1998 CAD *Proc. IEEE* **86** 1611

[4] Aluru N R and White J 1997 *Sensors and Actuators* A **58** 1

[5] Gillbert J R, Legtenberg R and Senturia S D 1995 *Proc. IEEE MEMS* 122

[6] Fang Y, Huang Q and Li W 2008 *Chin. Phys.* B **17** 1709

[7] Li G and Aluru N R 2002 *IEEE J. Microelectromech. Syst.* **11** 245

[8] Li G and Aluru N R 2001 *Sensors and Actuators* A **91** 278

[9] Li G, Paulino G H and Aluru N R 2003 *Comput. Methods Appl. Mech. Engrg.* **192** 2355

[10] Younis M I, Abdel-Rahman E M and Nayfeh A 2003 *IEEE J. Microelectromech. Syst.* **12** 672

[11] Younis M I, Abdel-Rahman E M and Nayfeh A 2002 *J. Micromech. Microeng.* **12** 759

[12] Tilmans H A C 1997 *J. Micromech. Microeng.* **7** 285

[13] Gabbay L D, Mehner J E and Senturia S D 2000 *IEEE J. Microelectromech. Syst.* **9** 262

[14] *ANSYS 7.0 Documetation——Coupled-Field Analysis* Guide ANSYS Inc 2002

[15] Meirovitch L 1975 *Elements of Vibration Analysis* (New York: McGraw-Hill)

[16] Shi F, Ramesh R and Mukherjee S 1995 *Commun. Numeric Meth. Eng.* **11** 691

[17] Katsikadelis J T 2002 *Boundary Elements Theory and Applications* (Oxford: Elsevier Science Ltd)

[18] Brebbia C A, Telles J C F and Wrobel L C 1984 *Boundary Element Techniques* (Berlin: Springer-Verlag)